A Climate Perspective of the Quasi-Stationary Front in Southwestern China: Structure, Variation and Impact

Danping Cai
Schoolf of Atmospheric Sciences, Nanjing University
Xiu-Qun Yang (xqyang@nju.edu.cn)
Nanjing University https://orcid.org/0000-0003-3716-9152
Lingfeng Tao
School of Atmospheric Sciences, Nanjing University
Weiping Wang
Guizhou Climate Center, Guiyang
Hongming Yan
Yunnan Climate Center, Kunming

Research Article

Keywords: quasi-stationary front, cloud and rainfall, subseasonal variation, Yunnan-Guizhou Plateau, southwestern China.

Posted Date: September 23rd, 2021

DOI: https://doi.org/10.21203/rs.3.rs-881120/v1

Version of Record: A version of this preprint was published at Climate Dynamics on January 25th, 2022.
See the published version at https://doi.org/10.1007/s00382-022-06151-1.

A climate perspective of the quasi-stationary front in southwestern China: structure, variation and impact

Danping Cai[a], Xiu-Qun Yang[a, b], Lingfeng Tao[a], Weiping Wang[c], and Hongming Yan[d]

[a] *CMA-NJU Joint Laboratory for Climate Prediction Studies, School of Atmospheric Sciences, Nanjing University, Nanjing 210023, China*

[b] *Southern Marine Science and Engineering Guangdong Laboratory (Zhuhai), Zhuhai 519082, China*

[c] *Guizhou Climate Center, Meteorological Bureau of Guizhou Province, Guiyang 550002, China*

[d] *Yunnan Climate Center, Meteorological Bureau of Yunnan Province, Kunming 650034, China*

Corresponding author address:

Dr. Xiu-Qun Yang, xqyang@nju.edu.cn

School of Atmospheric Sciences

Nanjing University, Nanjing 210023, China

Submitted to *Climate Dynamics*

September 5, 2021

Abstract

Yunnan-Guizhou quasi-stationary front (YGQSF) is a unique weather phenomenon that frequently occurs during winter half year over the Yunnan-Guizhou Plateau in southwestern China. Most of previous studies analyzed it only with synoptic cases. This study investigates the structure, variation, and impact of YGQSF from a climate perspective, using long-term high-resolution atmospheric reanalysis and high-density station records for 1981-2016. An objective method quantifying YGQSF is proposed and three indexes are defined to measure the intensity, frequency, and location of YGQSF, respectively, with the horizontal gradient of air potential temperature at a terrain-following level of sigma 0.995. With these indexes, climatological structure, subseasonal variability as well as climatic impact of YGQSF are comprehensively examined. In climatology, YGQSF as a north-south-oriented low-level front is found to occur the most frequently during January-February-March (JFM), determined predominately by the coldness from the east of the front. The structure of YGQSF identified essentially reflects an obstruction of high-terrain Yunnan (the western part of the plateau) to the low-level cold air mass, which makes near-surface cold northeasterly winds cease westward intruding and veer upward over relatively low-terrain Guizhou, transporting moisture upward and forming low clouds. A sharp climate contrast is thus formed between two sides of YGQSF: cold, sunless, and continuously rainy Guizhou versus warm and sunny Yunnan. Furthermore, YGQSF features significant subseasonal variations with periods at around 30d and 60d largely in its intensity. Anomalously strong YGQSF events which are caused 75% by the cold anomaly from the east but less than 17% by the warm anomaly from the west yield different anomalous structures, but consistently amplify the sharp climate contrast between Yunnan and Guizhou.

Keywords: quasi-stationary front; cloud and rainfall; subseasonal variation; Yunnan-Guizhou Plateau; southwestern China.

1 Introduction

The quasi-stationary front is a unique weather phenomenon that frequently occurs during winter half year in southwestern China. Since this front is found to be always anchored in the Yunnan-Guizhou Plateau, a specific region with the Tibetan Plateau on its northwestern side and vast plains and hills on its eastern side (Fig. 1), it is usually referred to as the Yunnan-Guizhou quasi-stationary front (YGQSF). The topographic altitude of the Yunnan-Guizhou Plateau is 2~4 km, and the topography of Yunnan Province (the western part of Yunnan-Guizhou Plateau) is generally 1 km higher than that of Guizhou Province (the eastern part of Yunnan-Guizhou Plateau). When a cold air mass moving from the eastern plains and hills to the Yunnan-Guizhou Plateau meets a warm air mass moving from the western plateau, a quasi-stationary front is thus formed on the slope roughly between the two provinces. As one of key weather systems in southwestern China during winter half year, YGQSF is characterized by a sharp contrast of the weather conditions on its two sides, with severe cold, cloudy weather and freezing disasters in Guizhou but mild sunny weather in Yunnan, (Zhao et al. 2008; Yang et al. 2011; Zhou et al. 2011; Deng et al. 2012; Du et al. 2015; Tao et al. 2018).

Previous case studies identified the synoptic structure of YGQSF and found some common features existing among individual cases. YGQSF is roughly a north-south-orientated front located between Yunnan and Guizhou, with a vertical

height below 700 hPa (Egger and Tao 1992; Duan et al. 2002; Du et al. 2007a). Properties of the air masses on both sides of the front are in huge difference, with warm and dry conditions in the west but cold and wet conditions in the east (Duan et al. 2002, Du et al. 2007a). In addition, a clock-wise secondary zonal circulation exists in the east of YGQSF (Li 1999; Duan et al. 2002; Lu et al. 2019; Xiao et al. 2019). However, the structure of YGQSF also exhibits some differences from event to event. In some cases, a thermal inversion layer appears in the east of YGQSF (Li et al. 2009; Yang et al. 2009; Du and Lan 2010; Du et al. 2010; Du et al. 2014), while in other cases it is absent (Duan et al. 2002; Du and Lan 2010). This demonstrates that the characteristics of YGQSF derived from synoptic events depend on the selection of those events. In order to comprehensively capture the general characteristics of YGQSF, it is necessary to conduct the investigation from a climate perspective.

A few previous studies revealed the occurrence frequency of YGQSF by simply counting the number of YGQSF events. For examples, Du et al. (2007b) indicated that the YGQSF activity features a seasonal variation with a high occurrence frequency from December to May and a low frequency from June to November. Zhang et al. (2016) pointed out that the number of YGQSF events exhibits a decreasing trend from 1970 to 2009. It is worth noting that the YGQSF events defined in previous studies are identified empirically, which would induce the subjective uncertainties in quantifying YGQSF. Meanwhile, the statistical method used in previous studies is only for the occurrence frequency of YGQSF events but not for the frontal intensity, which would limit the comprehensive understanding of YGQSF and its variations.

Therefore, it is necessary to propose a more objective method to identify and quantify YGQSF. During the past decades, how to objectively identify fronts on the isobaric surface were widely discussed (Renard and Clarke 1965; Hewson, 1998; McCann and Whistler 2001; Hope et al. 2014). Based on the thermodynamic method proposed by Hewson (1998), Zhao et al. (2019) recognized three YGQSF events occurring at 850 hPa in early 2008. However, this single-isobaric-surface-based method is not applicable anymore when YGQSF moves westward to higher land. The detection methods relying on the isobaric surface are not suitable for YGQSF due to the huge topographic change in Yunnan-Guizhou Plateau. Considering the unique topography, Duan et al. (2017) provided a method especially for identifying YGQSF, but the criteria used in this method are still overly dependent on the subjective experience from weather analysis. How to objectively identify and quantify YGQSF is still an open question.

This study intends to present a comprehensive investigation on the structure, variation and impact of YGQSF from a climate perspective. Specifically, this study defines three indexes to quantitatively characterize YGQSF based on both topographic features of Yunnan-Guizhou Plateau and objective criteria. With these quantified indexes, the climatological structure, the subseasonal variability as well as the climatic impact of YGQSF are examined with long-term high-resolution atmospheric reanalysis data and observations from high-density stations.

The rest of the paper is structured as follows. Section 2 describes the dataset used. Section 3 defines three indexes to quantify the intensity, frequency, and location of

YGQSF, respectively. In section 4, the climatological characteristics of wintertime YGQSF are revealed. The atmospheric anomalies associated with the subseasonal variation of the YGQSF intensity are presented in section 5. The final section is devoted to summary and discussion.

2 Datasets used

The National Center for Environmental Prediction (NCEP) Climate Forecast System Reanalysis (CFSR) dataset with horizontal resolution of $0.5^o \times 0.5^o$ for the period of 1981-2016 is used to analyze the structure and variation of YGQSF and associated atmospheric circulation. Daily atmospheric variables taken from the reanalysis include air temperature, wind velocity, and specific humidity at 27 standard pressure levels from 1000 hPa to 100 hPa, and air potential temperature and wind velocity at the level of sigma 0.995. In addition, the daily cloud cover fraction and specific cloud liquid water content at 27 standard pressure levels from 1000 hPa to 100 hPa, obtained from ERA-Interim reanalysis with the horizontal resolution of $0.5^o \times 0.5^o$ for 1981-2016 of European Centre for Medium-Range Weather Forecasts, are used to analyze the cloud distribution related to YGQSF.

The dataset of records at more than 2000 stations in China including daily maximum air temperature, daily sunshine duration, and daily precipitation for 1981-2016, taken from the National Meteorological Information Center of the China Meteorological Administration, is used to analyze the climatic impact of YGQSF. According to the precipitation from this dataset, a new variable, the rainfall frequency, is defined to describe the continuously rainy weather. A day with precipitation more

than 0.1 mm is defined as a rainy day (Wang et al. 2017), and a 7-day window mean of the number of rainy days is defined as the rainfall frequency.

In this study, the wintertime refers to January-to-March (JFM), since YGQSF is the strongest and the most frequently occurring during this period. To extract subseasonal variabilities, removals of firstly the climatological annual cycle and then the yearly JFM mean (i.e., interannual signals) are applied to all the data to get daily anomalies.

3 Indexes quantifying YGQSF

Considering the large terrain height difference between the eastern and western parts of Yunnan-Guizhou Plateau, it is appropriate to delineate YGQSF with air potential temperature and its gradient at terrain-following levels, which can avoid the effect of vertical temperature lapse rate induced by the terrain (Duan et al. 2017, Duan et al. 2018b). In this study, the horizontal air potential temperature gradient at the level of sigma 0.995 is calculated in terms of $|\nabla_h \theta| = \sqrt{\left(\frac{\partial \theta}{\partial x}\right)^2 + \left(\frac{\partial \theta}{\partial y}\right)^2}$ to quantify the front.

Figure 2 shows the spatial distributions of climatological air potential temperature and its horizontal gradient at the level of sigma 0.995 over the Yunnan-Guizhou Plateau (labeled by the black box in Fig. 1) in January, April, July, and October, respectively. Dense contours of air potential temperature and its large gradients mainly exist meridionally between 103°E and 106°E in the whole year, with the maximum gradient in January and the minimum gradient in July. The air potential temperature in the west is higher than that in the east. This result provides a clear evidence that YGQSF is a

155 climatological front north-south oriented between Yunnan and Guizhou and is the
156 most significant in winter. Thus, YGQSF can be climatologically recognized as the
157 large horizontal air potential temperature gradients at the level of sigma 0.995 in the
158 region of 23.5°N-27°N, and 103°E-106°E, labeled by the green box in Fig. 2. Given
159 those facts, three daily indexes are objectively defined in this study to quantify the
160 intensity, frequency, and location of YGQSF, respectively, in terms of the air potential
161 temperature gradients at the level of sigma 0.995.

162 An index quantifying the YGQSF intensity is defined as the regionally-averaged
163 horizontal air potential temperature gradients that are greater than a threshold value
164 within the frontal zone (the green box in Fig. 2). Considering the climatological
165 distribution of the gradients in different seasons (Fig. 2), the threshold value is set to
166 be 1.5 K/100km. The concrete formula for calculating the daily intensity index of
167 YGQSF, *its*, is written as:

168 $$its_i = \frac{1}{N_i}\sum_{j=1}^{N_i}\left|\nabla_h\theta_{ij}\right|, \quad (1)$$

169 where $\left|\nabla_h\theta_{ij}\right|$ is the horizontal air potential temperature gradient at the level of
170 sigma 0.995 with a criterion that the gradient must be larger than 1.5×10^{-2} K km^{-1} at
171 the j^{th} grid point within the frontal zone in the i^{th} day, and N_i is the number of the total
172 grid point satisfying the criterion in the i^{th} day. A large *its* means a strong YGQSF, and
173 vice versa.

174 In order to measure the activity of YGQSF, an index quantifying the occurrence
175 frequency of YGQSF is defined as the 7-day window mean of the number of days
176 with the YGQSF intensity index (*its*) greater than 3 K/100km (the rounding of

whole-year-mean climatological YGQSF intensity), which is written as:

$$frq_i = \frac{1}{7}\sum_{l=i-3}^{i+3} k_l\,;\;\; k_l = \begin{matrix} 1 & its_l > 3 \\ 0 & its_l \le 3 \end{matrix}, \tag{2}$$

where k_l indicates if the l^{th} day is a strong-YGQSF day or not. If the *its* is greater than 3×10^{-2} K km^{-1} in the l^{th} day, then YGQSF is relatively strong and k_l is et to be 1, else k_l equals 0. Therefore, a large *frq* means that YGQSF occurs frequently and lasts long.

Here the location of YGQSF is focused on its longitude shift as YGQSF generally is a north-south-orientated front (Fig. 2). The longitude index is defined as a weighted-average of the longitude with respect to the horizontal air potential temperature gradients at the level of sigma 0.995 greater than 1.5×10^{-2} K km^{-1} within the frontal zone, which is written as:

$$lon_i = \frac{\sum_{j=1}^{N_i}|\nabla_h\theta_{ij}|\times LON_{ij}}{\sum_{j=1}^{N_i}|\nabla_h\theta_{ij}|}, \tag{3}$$

where LON_{ij} is the longitude of j^{th} grid point within the frontal zone with $|\nabla_h\theta_{ij}|$ greater than 1.5×10^{-2} K km^{-1} in the i^{th} day. The *lon* denotes the YGQSF location in longitude, and a large *lon* means that YGQSF has an eastward shift.

4 Climatological characteristics of YGQSF

In terms of above defined three indexes, the climatological seasonal evolution of YGQSF can be analyzed in detail. Figure 3 shows the climatological annual cycles of the YGQSF indexes, as well as the regional-averaged air potential temperatures at the level of sigma 0.995 on the western and eastern sides of YGQSF, respectively. The intensity and frequency indexes of YGQSF are in phase with each other, with an increase from August to January and a decrease from February to July (Figs. 3a, b).

198 Both of these two indexes peak at around January to March (JFM), indicating that
199 YGQSF is the strongest, the most frequently occurring, and the longest-lasting during
200 JFM, consistent with the result of counting the number of individual YGQSF events
201 (Du et al. 2007b). During the increase (decrease) of YGQSF intensity and frequency
202 from August to January (from February to July), the cooling (warming) on the eastern
203 side (blue line in Fig. 3d) is more rapid than that on the western side (red line in Fig.
204 3d). These results demonstrate that it is the cold air in the east that plays the leading
205 role in the seasonal evolution of YGQSF. As for the longitude location of YGQSF, it
206 stays at around 104.6^{o}E in the whole year, with a slight west-east shift within 0.5^{o}
207 longitudes (Fig. 3c). Although the zonal movements of YGQSF are found on a
208 synoptic timescale (Zhang and Duan 2018), the quasi-stationary characteristic of the
209 front found here is prominent in climatology.

210 During JFM when YGQSF is the strongest and the longest-lasting, the climate in
211 the Yunnan-Guizhou region is significantly associated with the front. Figure 4 shows
212 horizontal distributions of the climatological JFM daily maximum air temperature,
213 sunshine duration, precipitation, and rainfall frequency according to the high-density
214 station records in southern China. A striking feature is that the wintertime climates in
215 Yunnan and Guizhou are dramatically different although their geographic locations
216 are both at around 25^{o}N. Compared to warm and sunny Yunnan, Guizhou is much
217 colder (Fig. 4a) and sunless (Fig. 4b), with more precipitation (Fig. 4c) and more
218 frequent raining (Fig. 4d). In eastern China, the rainfall frequency are comparable to
219 that in Guizhou (Fig. 4d), but the precipitation is much larger (Fig. 4c). This result is

supported by Li and Yu (2014) which demonstrated that the precipitation over the Yunnan-Guizhou Plateau is more concentrated in weak events compared to that in southeastern China. The climate related to YGQSF is distinct from that in other regions, showing a sharp contrast between the two sides of YGQSF: Guizhou in the east is invariably cold, sunless, and rainy, while Yunnan in the west is always warm and sunny.

According to previous case analyses on synoptic timescale, the vertical structure of YGQSF plays an important role in the extreme weather near the front (Yang et al. 2009; Du et al 2014; Lu et al 2019; Xiao et al. 2019). Similarly, the above climate impact of YGQSF during JFM is closely related to its climatological vertical structure. Figure 5 presents vertical distributions of the climatological JFM air potential temperature and its horizontal gradients, zonal and vertical wind, specific humidity, fraction of cloud cover, and cloud water content averaged between 23.5^{o}N and 27^{o}N over the Yunnan-Guizhou Plateau, respectively. As shown in Fig. 5a, the climatological air potential temperature shows a contrast of the warm west versus the cold east above the terrain and below 700 hPa, with the large gradients located between 104^{o}E and 105^{o}E. This indicates that the climatological YGQSF is a shallow system below 700 hPa. The near-surface easterly wind below 850 hPa in the eastern part of the plateau veers upward due to the obstruction of the western higher terrain. Beyond that, the frontal zone is nearly controlled by the westerly wind at the upper layer (Fig. 5b). Most of the moistures concentrate in the lower troposphere to the east of YGQSF. A contrast of the dry west versus the wet east at the same altitude is found

242 above the terrain and below 700 hPa, with the strongest contrast at around 750 hPa
243 (Fig. 5c). Influenced by such a climatological configuration of ascending motion and
244 abundant moisture in the east of YGQSF, the fraction of cloud cover and cloud liquid
245 water content are also large there (Figs. 5d, e). It is such low-level clouds that cause
246 the sunless and continuously rainy climate in Guizhou.

247 The structure of YGQSF is a local embodiment in this region of the large-scale
248 atmospheric circulation. In previous studies focusing on synoptic timescale, the
249 formation of YGQSF is found to be influenced by the terrain height difference
250 between the eastern and western parts of the Yunnan-Guizhou Plateau (Wang et al.
251 2009; Suo and Ding 2016; Duan et al. 2018a) and the large-scale atmospheric
252 circulation including the midlatitude trough/ridge and blocking (Du et al. 2014; Zhang
253 and Duan 2017; Suo et al. 2018), the Hadley and Ferrel Cells (Du et al. 2007a), the
254 Southern Branch Trough and the Western Pacific Subtropical High (Zhang et al. 2016).
255 To climatologically analyze the large-scale atmospheric circulation associated with
256 the structure of YGQSF discussed above, Figure 6 shows the climatological JFM air
257 potential temperature and horizontal wind at sigma 0.995 and at 750 hPa, as well as
258 the specific humidity flux and its divergence at 850 hPa and 750 hPa over East Asia.
259 At sigma 0.995, the East Asian continent is mainly controlled by a surface cold high,
260 accompanied by the southward intrusion of cold air from the midlatitudes into
261 southern China. Located at the southwestern end of the surface cold high, the eastern
262 part of Yunnan-Guizhou Plateau is influenced by the cold northeasterly wind. Besides,
263 the southwesterly wind in the east of the Southern Branch Trough advects the warm

air from the low-latitudes to the western part of the plateau (Fig. 6a). Due to the obstruction of the terrain, the cold northeasterly wind accumulates and veers upward in the eastern part of Yunnan-Guizhou Plateau and confronts the warm southwesterly wind in the western part, forming the climatological YGQSF. It is worth noting that the southwesterly warm wind at 750 hPa originating from the Southern Branch Trough and the Western Pacific Subtropical High dominantly prevails over the Yunnan-Guizhou Plateau (Fig. 6b), without any horizontal advection of cold air. This demonstrates that the climatological YGQSF is a shallow system generated by the large-scale circulation near the surface. As for the moisture transport, at 750 hPa, where the specific humidity contrast between the west and east sides of YGQSF is the strongest (Fig. 5c), a divergence of specific humidity flux exists in the eastern part of the Yunnan-Guizhou Plateau (Fig. 6d), although the southwesterly winds in the east of the South Branch Trough and on the northwestern side of the Western Pacific Subtropical High transport moisture northeastward. However, at the lower altitude of 850 hPa, the moisture is transported northwestward and converges in the eastern part of the Yunnan-Guizhou Plateau (Fig. 6c). This implies that the strongest contrast of the dry west versus the wet east at 750 hPa is not contributed by the horizontal transportation of moisture, but due to its upward transportation from the lower altitude.

5 Subseasonal variation of YGQSF and associated atmospheric anomalies

With the YGQSF indexes defined in Section 3, a wavelet analysis is performed to investigate the characteristics of the YGQSF variation. The climatological

time-frequency distributions of the YGQSF intensity, frequency, and location are shown in Fig. 7, in which the climatological wavelet power spectrum is shaded and the occurrence ratio of the wavelet power exceeding 90% confidence level in all analyzed years is contoured. The YGQSF intensity is characterized by two separate wavelet power centers in JFM, corresponding to two principal periods of around 30-day and 60-day, respectively, with significance occurrence ratios both more than 20%. This indicates that the YGQSF intensity indeed exhibits significant subseasonal variation. As for the YGQSF frequency, large and significant subseasonal variation with the typical period of 30-60-day appears in November-December and April-May. However, its wavelet power is weak and insignificant during JFM when YGQSF exists almost steadily (Fig. 7b). The Longitude-location of YGQSF shows weak subseasonal variation in JFM with two typical periods the same as those of the intensity (Fig. 7c), indicating that the east-west shift of YGQSF is quite weak on the subseasonal time scale.

Considering the strong and significant subseasonal variation of the YGQSF intensity in JFM, the structure and climate impact of an anomalously strengthened YGQSF on the subseasonal time scale are analyzed below through composite analysis. A strong YGQSF (Str_YGQSF) event is defined if the subseasonal anomaly of the daily YGQSF intensity exceeds +1.5 standard deviation, and then 234 Str_YGQSF events are identified in JFM for 1981-2016. To depict the anomalous horizontal thermal structure of the intensified YGQSF, Figure 8a demonstrates composite air potential temperature anomalies and their horizontal gradients at the level of sigma

0.995 over the Yunnan-Guizhou Plateau for those Str_YGQSF events. The intensified YGQSF can be identified by the positive horizontal air potential temperature gradient anomalies. The distribution of the air potential temperature exhibits an anomalous cold-east and warm-west structure, with the cold anomaly in the east larger than the warm anomaly in the west, implying the leading role of the eastern cold anomaly in the enhancement of YGQSF on the subseasonal timescale.

It is recognized in Section 4 that the cold air and warm air respectively in the eastern and western parts of the Yunnan-Guizhou Plateau are induced by different large-scale circulation systems. Therefore, it is necessary to classify the Str_YGQSF events into the eastern cold anomaly-induced strong YGQSF cases (CE_YGQSF) and the western warm anomaly-induced strong YGQSF cases (WW_YGQSF). A CE_YGQSF event is defined if a Str_YGQSF event with $|\theta'_{west}|/|\theta'_{east}| < 2/3$, where θ'_{west} and θ'_{east} represent the regional mean of air potential temperature anomaly at the level of sigma 0.995 within a western region (23.5°N-27°N, 99°E-104.5°E) and an eastern region (23.5°N-27°N, 104.5°E-110°E), respectively. A WW_YGQSF event is defined if a Str_YGQSF event with $|\theta'_{west}|/|\theta'_{east}| > 3/2$. In terms of these definitions, 169 CE_YGQSF events (around 75% of Str_YGQSF) and 34 WW_YGQSF events (no more than 17% of Str_YGQSF) are distinguished. The huge difference between numbers of these two kinds of Str_YGQSF events implies that the subseasonal enhancement of YGQSF is largely determined by the cold anomaly in the east. Anomalous horizontal thermal structures for CE_YGQSF and WW_YGQSF are shown in Figs. 8b, c, respectively. It is obvious that the location

of the positive horizontal air potential temperature gradient anomaly is slightly shifted westward in CE_YGQSF relative to that in WW_YGQSF, indicating that the strong eastern cold anomaly tends to induce the westward shift of anomalously enhanced YGQSF.

In order to clarify anomalous vertical structure of subseasonally intensified YGQSF, Figure 9 gives longitude-altitude sections of composite anomalies of air potential temperature, zonal and vertical wind, specific humidity, cloud cover fraction, and cloud liquid water content averaged between 23.5^{o}N and 27^{o}N over the Yunnan-Guizhou Plateau for three kinds of categorized strong YGQSF events. For the Str_YGQSF events, i.e., the total strong YGQSF events (left panels of Fig. 9), a considerable cold anomaly exists below 800 hPa in the eastern low-terrain region (east of 104.5^{o}E), compared to a relatively weak warm anomaly in the western high-terrain region (Fig. 9a). Above 800 hPa the whole plateau is controlled by the anomalous westerly wind, while below 800 hPa the anomalous easterly wind occurs in the eastern region and veers upward to around 700 hPa (Fig. 9d), strengthening the climatological circulation. Such an anomalous ascending motion enhances the upward moisture transportation, leading to an anomalous structure in moisture with the upper-level wet anomaly centered at 750 hPa and the lower-level dry anomaly below 800hPa (Fig. 9g). The eastern anomalous ascending motion also contributes to a positive cloud cover anomaly as well as a positive cloud water content anomaly below 600 hPa (Figs. 9j, m).

As two subsets of Str_YGQSF, anomalous vertical structures for CE_YGQSF

352 and WW_YGQSF are basically similar to that of Str_YGQSF, but differences are also
353 found, as shown in central and right panels of Fig. 9, respectively. Firstly, a stronger
354 cold anomaly expands more westward to 104°E and more upward to 750 hPa for
355 CE_YGQSF (Fig. 9b), while a stronger warm anomaly expands more eastward and
356 the cold anomaly is restricted to the east of 106°E and below 850 hPa for
357 WW_YGQSF (Fig. 9c). Secondly, the anomalous easterly wind and ascending motion
358 in the east are stronger and extend higher for CE_YGQSF (Fig. 9e) than for
359 WW_YGQSF (Fig. 9f), transporting more moisture upward. Consequently, the
360 eastern dry anomaly is stronger and extends more upward to 800 hPa for CE_YGQSF
361 (Fig. 9h), comparing with the weaker one below 900 hPa in WW_YGQSF (Fig. 9i).
362 Meanwhile, positive cloud cover and cloud water content anomalies in the east
363 expand upward to 600 hPa for CE_YGQSF (Figs. 9k, n), which is significantly higher
364 than those to 700 hPa for WW_YGQSF (Figs. 9l, o). Besides, the anomalous westerly
365 wind over the plateau above the near-surface is stronger for WW_YGQSF (Fig. 9f)
366 than for CE_YGQSF (Fig. 9e), promoting more moisture supply for the eastern region
367 by stronger anomalous horizontal moisture transportation. Therefore, the moistening
368 and the increased cloud cover and cloud water content are more significant in the east
369 for WW_YGQSF (Figs. 9i, l, and o). In addition, an apparent anomalous descending
370 motion in the west is found for WW_YGQSF (Fig. 9f), while it is invisible for
371 CE_YGQSF (Fig. 9e), which leads to a stronger negative cloud cover and cloud water
372 content anomaly in the west for WW_YGQSF (Figs. 9 l, o).
373 Above anomalous structure for a subseasonally enhanced YGQSF has climate

374 impacts in this region. Figure 10 shows composite anomalies of daily maximum air
375 temperature, sunshine duration, precipitation, and rainfall frequency over Yunnan and
376 Guizhou for Str_YGQSF, CE_YGQSF, and WW_YGQSF, respectively. When
377 YGQSF is enhanced, as an impact of the anomalous warm-west and cold-east
378 structure and the increased cloud cover in the east, Guizhou is anomalously cold (Fig.
379 10a), short of sunshine (Fig. 10d), and continuously rainy (Figs. 10g, j), while Yunnan
380 is anomalously warm (Fig. 10a) and sunny (Figs. 10d, g, and j), largely enhancing the
381 climatological contrast between the two provinces. As for the different climate
382 impacts of CE_YGQSF and WW_YGQSF, it can be seen that the stronger cold
383 anomaly and thicker positive cloud cover anomaly in the east contribute to the much
384 colder (Figs. 10b, c) and cloudier (Figs. 10e, f) Guizhou for CE_YGQSF; the stronger
385 warm anomaly and negative cloud cover anomaly in the west lead to the warmer (Figs.
386 10b, c) and sunnier (Figs. 10e, f, h, i, k and l) Yunnan for WW_YGQSF. It is worth
387 noting that the positive rainfall frequency anomalies in Guizhou for CE_YGQSF and
388 WW_YGQSF are basically in the same magnitude (Figs. 10k, l). This is probably
389 because the eastern cloud cover for CE_YGQSF is thicker but contains less moisture,
390 while that for WW_YQSF is thinner but contains more moisture.

391 **6 Summary and discussion**

392 YGQSF is a unique synoptic phenomenon that frequently occurs during winter
393 half year over the Yunnan-Guizhou Plateau in southwestern China and considerably
394 affects local weather and climate in this region. Most of previous studies analyzed it
395 only based on individual cases. This study extends the investigation to a climate

perspective of the structure, variation, and impact of YGQSF, using long-term high-resolution atmospheric reanalysis data and observations of high-density stations for 1981-2016. Considering the terrain height difference between the western and eastern parts of the Yunnan-Guizhou Plateau, an objective method quantifying YGQSF is proposed and three indexes are defined to measure the intensity, frequency, and location of YGQSF, respectively, with the horizontal air potential temperature gradient at the level of sigma 0.995, a terrain-following level, avoiding the effect of vertical temperature lapse rate induced by the terrain. With these quantified indexes, the climatological structure, the subseasonal variability as well as the climatic impact of YGQSF are comprehensively examined.

In climatology, YGQSF is found to the most frequently occur and be the strongest during JFM, which is determined predominately by the coldness from the east of the front. It is a north-south-oriented front with an averaged location at around 104.6^{o}E and a very slight zonal movement in the whole year.

Based on the results identified from this study, a summarized schematic diagram for the climatological structure of YGQSF during winter half year is shown in Fig. 11a. The cold northeasterly winds from the surface cold high in East Asia are impeded by the high-terrain western part of the Yunnan-Guizhou Plateau, leading to an accumulation and an ascent of cold air coming from the low-terrain eastern part of the plateau. Thus, moistures are transported upward from the near-surface to 750 hPa and low clouds are formed there. Meanwhile, the ascending cold air turns eastward at around 750 hPa, merging into the warm southwestern winds originating from the east

418 of the South Branch Trough and inducing a downstream moistening. Therefore,
419 although nearly located at the same latitude, Guizhou in the east of YGQSF is
420 invariably cold, sunless, and rainy while Yunnan in the west is always warm and
421 sunny, forming an intense climate contrast in the two sides of the front.

422 Wavelet analysis shows that the intensity of YGQSF is characterized by
423 subseasonal variabilities with two significant principal periods at around 30-day and
424 60-day, respectively, during JFM. The subseasonal cold (warm) anomaly alone in the
425 eastern (western) part of the Yunnan-Guizhou Plateau can enhance YGQSF, but the
426 former accounts for nearly 75% of the strong YGQSF events while the latter no more
427 than 17%. As shown in Figs. 11b, c, for whether the eastern cold anomaly-induced
428 strong YGQSF events (CE_YGQSF) or the western warm anomaly-induced strong
429 YGQSF events (WW_YGQSF), anomalous near-surface easterly winds are obstructed
430 by the western high terrain and veers upward in the eastern part. Thereby the upward
431 moisture transportation is anomalously strengthened, leading to an anomalous
432 upper-wet and lower-dry structure and an anomalous increase of clouds in the
433 low-level atmosphere. Controlled by the anomalous cold air mass and increasing
434 low-level clouds, Guizhou is anomalously cold, cloudy, and continuously rainy, while,
435 affected by the anomalous warm air mass, Yunnan is anomalously warm and sunny,
436 amplifying the climate contrast between two provinces.

437 Comparing with WW_YGQSF, the anomalous easterly wind and the ascending
438 motion of the eastern part are stronger and higher-reaching for CE_YGQSF, implying
439 more upward moisture transportation. Thus the anomalous upper-wet and lower-dry

structure and the anomalous increase of low-level clouds expand more westward and to higher troposphere in CE_YGQSF than in WW_YGQSF. Correspondingly, Guizhou is anomalously colder and cloudier. The anomalous westerly wind over the plateau above the near-surface is stronger in WW_YGQSF than in CE_YGQSF, promoting more moisture supply for the eastern part by stronger anomalous horizontal moisture transportation. Therefore, the anomalous increase of rainfall frequency of Guizhou in WW_YGQSF is comparable to that in CE_YGQSF. Besides, in WW_YGQSF there is an apparent anomalous descending motion in the western part that suppresses the cloud formation but is invisible in CE_YGQSF, inducing a much warmer and sunnier Yunnan directly in WW_YGQSF.

Climatologically, YGQSF is a local embodiment in this specific region of large-scale atmospheric circulation. Inferentially, the subseasonal variabilities of YGQSF are induced by the subseasonal variations of relevant large-scale atmospheric circulation. Since the YGQSF anomalies are majorly caused by the cold air activity, it is of great importance to further investigate subseasonal variations of the mid- and high-latitude atmospheric circulation determining the cold air activity in East Asia for understanding and predicting the YGQSF anomalies, although it is still a challenging issue to be solved.

Acknowledgements

This work is jointly supported by the National Key R&D Program of China (2018YFC1505902) and the National Natural Science Foundation of China (41621005). We are also grateful for support from the Jiangsu Collaborative

462 Innovation Center for Climate Change. The CFSR data was provided by Research
463 Data Archive at the National Center for Atmospheric Research and is available at
464 http://dx.doi.org/10.5065/D69K487J. The ERA-Interim data was produced by ECMWF
465 and was obtained from https://apps.ecmwf.int/datasets/. The station records were provided
466 by the National Meteorological Information Center of the China Meteorological
467 Administration.
468

469 **References**

470 Deng, D. F., S. T. Gao, X. L. Du and W. H. Wu, 2012: A diagnostic study of freezing
471 rain over Guizhou, China, in January 2011. *Quarterly Journal of the Royal*
472 *Meteorological Society*, **138**, 1233-1244.

473 Du, X. L., S. T. Gao and F. Peng, 2014: Study of the 2011 freezing rain and snow
474 storm in Guizhou. *Chinese Journal of Atmospheric Sciences*, **38**, 61-72. (in
475 Chinese)

476 Du, X. L. and W. Lan, 2010: Contrastive analysis on frontal structure of
477 quasi-stationary front in two precipitation processes of Yunnan-Guizhou.
478 *Plateau Meteorology*, **29**, 1183-1195. (in Chinese)

479 Du, X. L., F. Peng and W. H. Wu, 2010: Distribution and cause on frequent freezing
480 rain zone in Guizhou. *Meteorological Monthly*, **36**, 92-97. (in Chinese)

481 Du, Z. J., Z. Y. Ding and S. Y. Zhang, 2007a: Analysis of atmospheric circulation and
482 structure of Yunnan-Guizhou quasi-stationary front during its evolution.
483 *Journal of Tropical Meteorology*, **23**, 284-292. (in Chinese)

484 Du, Z. J., Y. L. He, F. Xiong, X. H. Deng, K. Y. Shi and Q. Peng, 2015: Analysis on
485 the frontogenesis mechanism of Dian-Qian quasi-stationary front inducing
486 spring rainstorm in Guizhou Province. *Plateau Meteorology*, **34**, 357-367. (in
487 Chinese)

488 Du, Z. J., F. Xiong and J. W. Su, 2007b: Some statistical characteristics of Dian-Qian
489 quasi-stationary front during 2001 to 2003. *Journal of Meteorological*
490 *Research and Application*, **28**, 21-23. (in Chinese)

491 Duan, X., W. Duan and D. Xing, 2017: A study of objective determination method for
492 the Kunming quasi-stationary frontline. *Acta Meteorologica Sinica* **75**,
493 811-822. (in Chinese)
494 Duan, X., W. Duan, D. Xing and Y. N. Zhang, 2018a: The relationship between
495 Kunming quasi-stationary front and Yunnan-Guizhou Plateau terrain. *Plateau*
496 *Meteorology*, **37**, 137-147. (in Chinese)
497 Duan, X., Y. LI and X. D. Sun, 2002: The structure of Kunming quasi-stationary front.
498 *Plateau Meteorology*, **21**, 205-209. (in Chinese)
499 Duan, X., Y. N. Zhang and H. L. Liang, 2018b: A comparative analysis of the
500 Kunming quasi-stationary frontal position and frontogenesis function with
501 three different temperature and humidity parameters. *Chinese Journal of*
502 *Atmospheric Sciences*, **42**, 301-310. (in Chinese)
503 Egger, J. and Z. Y. Tao, 1992: A note on the dynamics of the quasi-stationary
504 Kunming front. *Meteorology and Atmospheric Physics*, **48**, 225-229.
505 Hewson, T. D., 1998: Objective fronts. *Meteorological Applications*, **5**, 37-65.
506 Hope, P., K. Keay, M. Pook, J. Catto, I. Simmonds, G. Mills, P. McIntosh, J. Risbey
507 and G. Berry, 2014: A Comparison of Automated Methods of Front
508 Recognition for Climate Studies: A Case Study in Southwest Western
509 Australia. *Monthly Weather Review*, **142**, 343-363.
510 Jong, P. C., 1947: Air mass and quasi-stationary surface in southwestern China.
511 *Journal of Science*, **29**, 339. (in Chinese)
512 Li, D. W., Q. Qiao and T. Wei, 2009: Analyses on the freezing rain and snow weather

513 circulation and vertical structure of southern China in early 2008. *Plateau*
514 *meteorology*, **28**, 1140-1148. (in Chinese)
515 Li, J. and R. C. Yu, 2014: Characteristics of Cold Season Rainfall over the Yungui
516 Plateau. *Journal of Applied Meteorology and Climatology*, **53**, 1750-1759.
517 Li, Y., 1999: Conditional symmetric instability and high-wind and hail accompanying
518 with Kunming quasi-stationary front. *Journal of Tropical Meteorology*, **15**, 3-5.
519 (in Chinese)
520 Lu, Y. B., S. Tan, Y. Min, J. Hu, H. H. Li, Y. J. Xu and Z. Y. Yang, 2019: The analysis
521 of extreme rainstorm process as influenced by the Bay of Bengal low and
522 Kunming quasi-stationary front in Yunnan. *Advances in Meteorological*
523 *Science and Technology*, **9**, 24-31. (in Chinese)
524 McCann, D. W. and J. P. Whistler, 2001: Problems and solutions for drawing fronts
525 objectively. *Meteorological Applications*, **8**, 195-203.
526 Renard, R. J. and L. C. Clarke, 1965: Experiments in numerical objective frontal
527 analysis. *Monthly Weather Review*, **93**, 547-556.
528 Suo, M. Q. and Y. H. Ding, 2016: The discovery and study of Kunming
529 quasi-stationary front. *Advances in Meteorological Science and Technology*, **6**,
530 6-16. (in Chinese)
531 Suo, M. Q., Y. H. Ding, Y. B. Lu, S. Tang, X. J. Fan and J. H. Li, 2018: Effects of
532 quasi-stationary fronts in southern China on large-scale freezing rain in winter.
533 *Acta Meteorologica Sinica*, **76**, 525-538. (in Chinese)
534 Tao, Y., X. Duan, Y. Yao, C. C. Duan, J. Z. Ren, Y. Chen and H. He, 2018: The

climate correlation analysis between the cold wave in Yunnan and Kunming quasi-stationary front. *Journal of Catastrophology*, **33**, 99-105. (in Chinese)

Wang, M., X. Duan, H. H. LI and R. Fu, 2009: A numerical study of the effect of terrain on Kunming quasi-stationary front (KQSF). *Meteorological Monthly*, **35**, 77-83. (in Chinese)

Wang, W. P., X. Q. Yang, Z. Q. Zhang and Z. P. Wu, 2017: The climatic characteristics and trends of rainy days over China. *Journal of the Meteorological Sciences*, **37**, 317-328. (in Chinese)

Xiao, Y. L., Z. X. Chi, R. Yan, Z. Y. Zhai and L. J. Liu, 2019: Comparative analysis of two torrential rain in the background of quasi-stationary front in Guizhou. *Mid-low Latitude Mountain Meteorology*, **43**, 1-8. (in Chinese)

Yang, G. M., D. Y. Mao and Q. Kong, 2009: Analysis of the frontal characteristics of the cryogenic freezing rain and snow weather. *Acta Meteorologica Sinica*, **67**, 652-665. (in Chinese)

Yang, J., C. Wang, F. Peng and D. W. Li, 2011: Characteristics of a persistent frontal fog event in low-latitude mountain area. *Meteorological Science and Technology*, **39**, 445-452. (in Chinese)

Zhang, J. H., W. C. Zhang, J. M. Zheng and T. Ma, 2016: Variation of Kunming quasi-stationary front and its effect analysis in winter during 1970-2009. *Plateau Meteorology*, **35**, 1298-1306. (in Chinese)

Zhang, J. W. and X. Duan, 2017: Comparative analysis of the typical cold processes influenced by Kunming quasi-stationary front. *Journal of Yunnan University*,

39, 798-809. (in Chinese)

Zhang, Y. N. and X. Duan, 2018: Structural characteristics of the advance, retreat and maintenance of Kunming quasi-stationary front in January. *Plateau Meteorology*, **37**, 1375-1387. (in Chinese)

Zhao, D., R. W. Yang, Y. Tao, W. K. Zhang and X. C. He, 2019: Objective detection of the Kunming quasi-stationary front. *Theoretical and Applied Climatology*, **138**, 1405-1418.

Zhao, L. N., Q. Y. Ma, G. M. Yang, X. R. Wang, L. Q. Zhao, X. D. Yang, H. Wu, Z. Wang, Z. M. Kang and D. Y. Mao, 2008: Disasters and its impact of a severe snow storm and freezing rain over southern China in January 2008. *Climatic and Environmental Research*, **13**, 556-566. (in Chinese)

Zhou, B. Z., L. H. Gu, Y. H. Ding, L. Shao, Z. M. Wu, X. S. Yang, C. Z. Li, Z. C. Li, X. M. Wang, Y. H. Cao, B. S. Zeng, M. K. Yu, M. Y. Wang, S. K. Wang, H. G. Sun, A. G. Duan, Y. F. An, X. Wang and W. J. Kong, 2011: The Great 2008 Chinese Ice Storm: Its Socioeconomic–Ecological Impact and Sustainability Lessons Learned. *Bulletin of the American Meteorological Society*, **92**, 47-60.

574 **Figure captions**

575 **Figure 1** Distribution of topographic altitude of southern China. Note that the black
576 box roughly represents the location of the Yunnan-Guizhou Plateau, and the west and
577 east black asterisks represent the location of Kunming (the provincial capital of
578 Yunnan) and Guiyang (the provincial capital of Guizhou), respectively.

579 **Figure 2** Horizontal distributions of climatological air potential temperature (contour,
580 units: K) and its horizontal gradient (shaded, units: 10^{-2} K km^{-1}) at the level of sigma
581 0.995 over the Yunnan-Guizhou Plateau in (a) January, (b) April, (c) July, and (d)
582 October, respectively, for 1981-2016. The red and blue boxes represent the western
583 (23.5°N-27°N, 99°E-104.5°E) and eastern (23.5°N-27°N, 104.5°E-110°E) parts of the
584 Yunnan-Guizhou Plateau, respectively; and the green box represents the frontal zone
585 of YGQSF (23.5°N-27°N, 103°E-106°E). The left (right) black asterisk represents
586 Kunming (Guiyang), as in Fig. 1.

587 **Figure 3** Climatological seasonal evolutions of daily (a) YGQSF intensity index
588 (units: 10^{-2} K km^{-1}), (b) YGQSF frequency index (units: %), (c) YGQSF location
589 index (units: °E), and (d) potential temperature at the level of sigma 0.995 averaged
590 over the western part (red line, units: K) and eastern part (blue line, units: K) of the
591 Yunnan-Guizhou Plateau, respectively, for 1981-2016. The red dash lines in (a), (b)
592 and (c) represent the climatological annual means.

593 **Figure 4** Horizontal distributions of climatological (a) daily maximum air
594 temperature (units: °C), (b) daily sunshine duration (units: hr day^{-1}), (c) daily
595 precipitation (units: mm day^{-1}), and (d) rainfall frequency (units: %) in southern China

596 during JFM for 1981-2016, based on the station records.

597 **Figure 5** Longitude-altitude sections averaged between 23.5°N-27°N of
598 climatological (a) air potential temperature (black contour, units: K) and its deviation
599 from the zonal mean between 99°E-110°E (shaded, units: K), and horizontal air
600 potential temperature gradient (green contour, units: 10^{-2} K km^{-1}), (b) zonal and
601 vertical wind vector (vector, units: m s^{-1}), (c) specific humidity (contour, units: g kg^{-1})
602 and its deviation from the zonal mean between 99°E-110°E (shaded, units: g kg^{-1}), (d)
603 fraction of cloud cover (shaded, units:%), and (e) specific cloud liquid water content
604 (shaded, units: 10^{-2} g kg^{-1}) over the Yunnan-Guizhou Plateau, during JFM for
605 1981-2016. The red line in (b) represents the zero line of climatological zonal wind
606 velocity. The gray shadings represent the topography, and the western and eastern
607 black asterisks represent the location of Kunming and Guiyang, respectively.

608 **Figure 6** Horizontal distributions of climatological air potential temperature (shaded,
609 units: K) and horizontal wind vector (vector, units: m s^{-1}) at (a) the level of sigma
610 0.995 and (b)750 hPa, as well as specific humidity flux (vector, units: 10^{2} g kg^{-1} m s^{-1})
611 and its divergence (shaded, units: 10^{-7} g kg^{-1} s^{-1}) at (c) 850 hPa and (d) 750 hPa over
612 East Asia, during JFM for 1981-2016. The black boxes represent the location of the
613 Yunnan-Guizhou Plateau.

614 **Figure 7** Wavelet power spectrum (shaded) averaged from 1981 to 2016 and
615 occurrence ratios (contours, units: %) of the wavelet power exceeding 90%
616 confidence level (regular chi-square test) in 1981-2016 for standardized (a) intensity
617 index, (b) frequency index, and (c) location index of YGQSF. The square-filled

618 shadings are the cones of influence.

619 **Figure 8** Horizontal distributions of composite anomalies of air potential temperature
620 (contour, units: K) and its horizontal gradient (shaded, units: 10^{-2} K km^{-1}) for (a)
621 Str_YGQSF, (b) CE_YGQSF, and (c) WW_YGQSF at the level of sigma 0.995 over
622 the Yunnan-Guizhou Plateau. The dots indicate the regions exceeding 95% confidence
623 level with the Student's t-test. The left (right) black asterisk represents Kunming
624 (Guiyang), as in Fig. 1..

625 **Figure 9** Longitude-altitude sections averaged between 23.5°N-27°N of composite
626 anomalies of (a, b, c) air potential temperature (shaded, units: K), (d, e, f) zonal wind
627 velocity (shaded, units: m s^{-1}) and zonal and vertical wind vector (vector, units: m s^{-1}),
628 (g, h, i) specific humidity (units: g kg^{-1}), (j, k, l) fraction of cloud cover (units: %),
629 and (m, n, o) specific cloud liquid water content (units: 10^{-2} g kg^{-1}) for Str_YGQSF
630 (left panels), CE_YGSQF (central panels), and WW_YGQSF (right panels),
631 respectively. The dots indicate the regions exceeding 95% confidence level with the
632 Student's t-test.

633 **Figure 10** Horizontal distributions of composite anomalies of (a, b, c) daily maximum
634 air temperature (units: °C), (d, e, f) daily sunshine duration (units: hr day^{-1}), (d, h, i)
635 daily precipitation (units: mm day^{-1}), and (j, k, l) rainfall frequency (units: %) for
636 Str_YGQSF (left panels), CE_YGQSF (central panels), and WW_YGQSF (right
637 panels) in Yunnan and Guizhou Provinces, based on the station records. Note that only
638 the values exceeding 95% confidence level with the Student's t-test are plotted.

639 **Figure 11** Schematic diagrams for the structures of (a) climatological YGQSF, (b)

640 CE_YGQSF, and (c) WW_YGQSF.

641

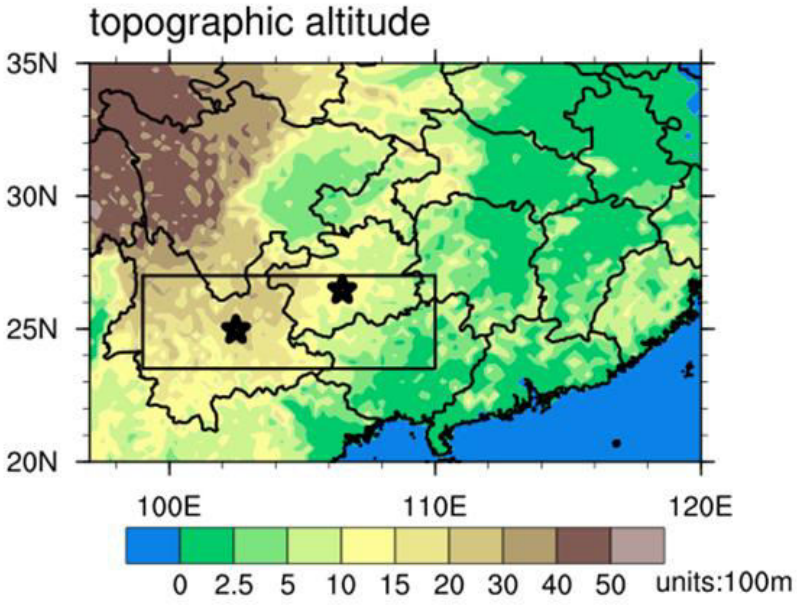

642

643 **Figure 1** Distribution of topographic altitude of southern China. Note that the black

644 box roughly represents the location of the Yunnan-Guizhou Plateau, and the west and

645 east black asterisks represent the location of Kunming (the provincial capital of

646 Yunnan) and Guiyang (the provincial capital of Guizhou), respectively.

647

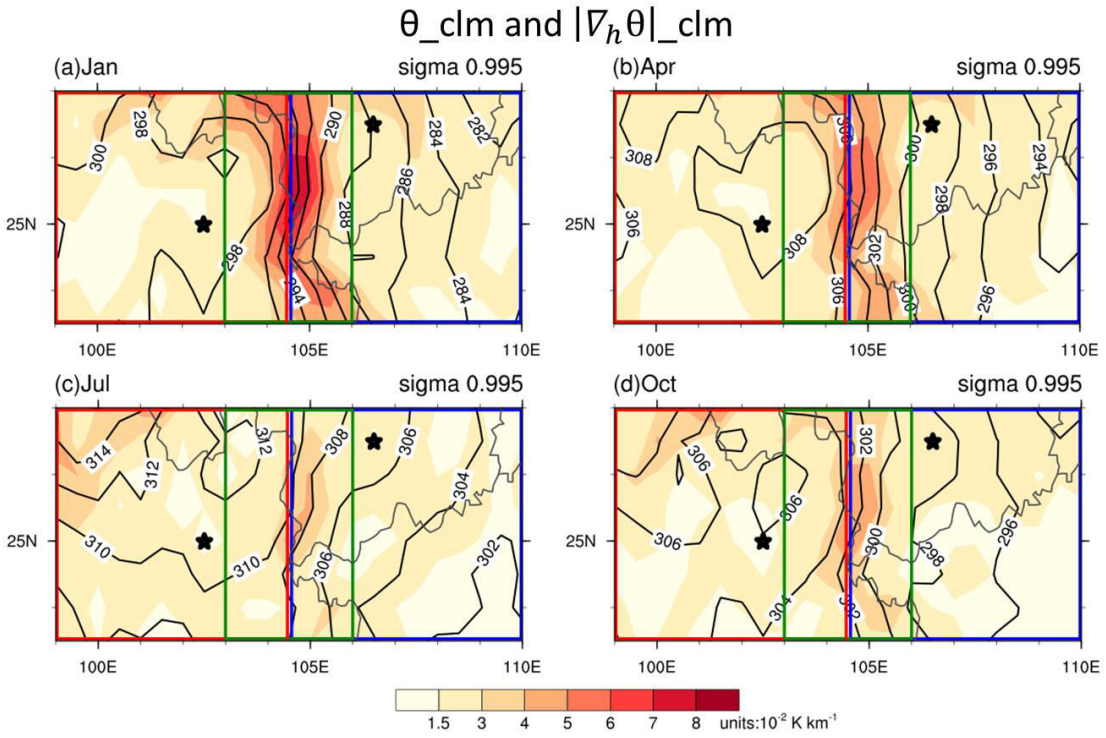

Figure 2 Horizontal distributions of climatological air potential temperature (contour, units: K) and its horizontal gradient (shaded, units: 10^{-2} K km^{-1}) at the level of sigma 0.995 over the Yunnan-Guizhou Plateau in (a) January, (b) April, (c) July, and (d) October, respectively, for 1981-2016. The red and blue boxes represent the western (23.5°N-27°N, 99°E-104.5°E) and eastern (23.5°N-27°N, 104.5°E-110°E) parts of the Yunnan-Guizhou Plateau, respectively; and the green box represents the frontal zone of YGQSF (23.5°N-27°N, 103°E-106°E). The left (right) black asterisk represents Kunming (Guiyang), as in Fig. 1.

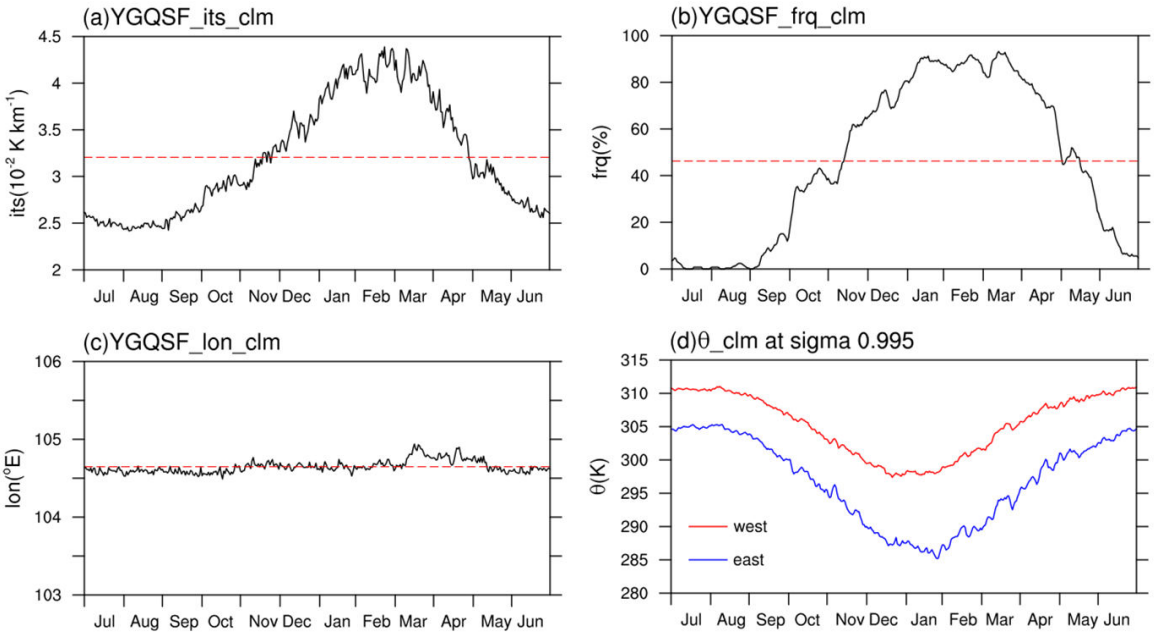

Figure 3 Climatological seasonal evolutions of daily (a) YGQSF intensity index (units: 10^{-2} K km^{-1}), (b) YGQSF frequency index (units: %), (c) YGQSF location index (units: ^{o}E), and (d) potential temperature at the level of sigma 0.995 averaged over the western part (red line, units: K) and eastern part (blue line, units: K) of the Yunnan-Guizhou Plateau, respectively, for 1981-2016. The red dash lines in (a), (b) and (c) represent the climatological annual means.

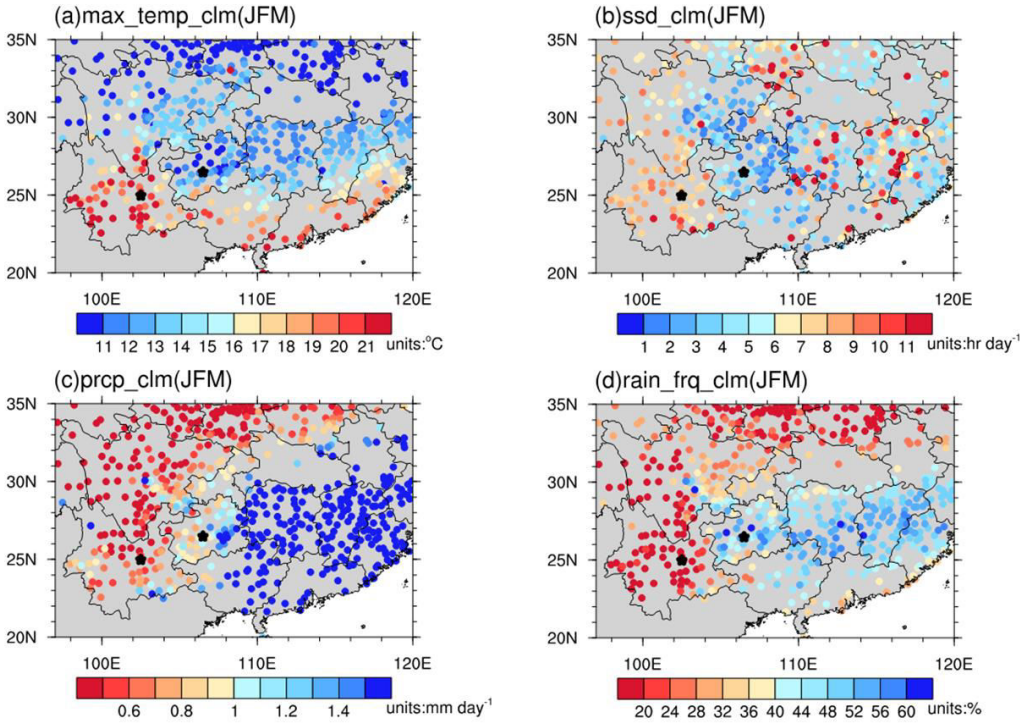

665

666 **Figure 4** Horizontal distributions of climatological (a) daily maximum air

667 temperature (units: ^{o}C), (b) daily sunshine duration (units: hr day^{-1}), (c) daily

668 precipitation (units: mm day^{-1}), and (d) rainfall frequency (units: %) in southern China

669 during JFM for 1981-2016, based on the station records.

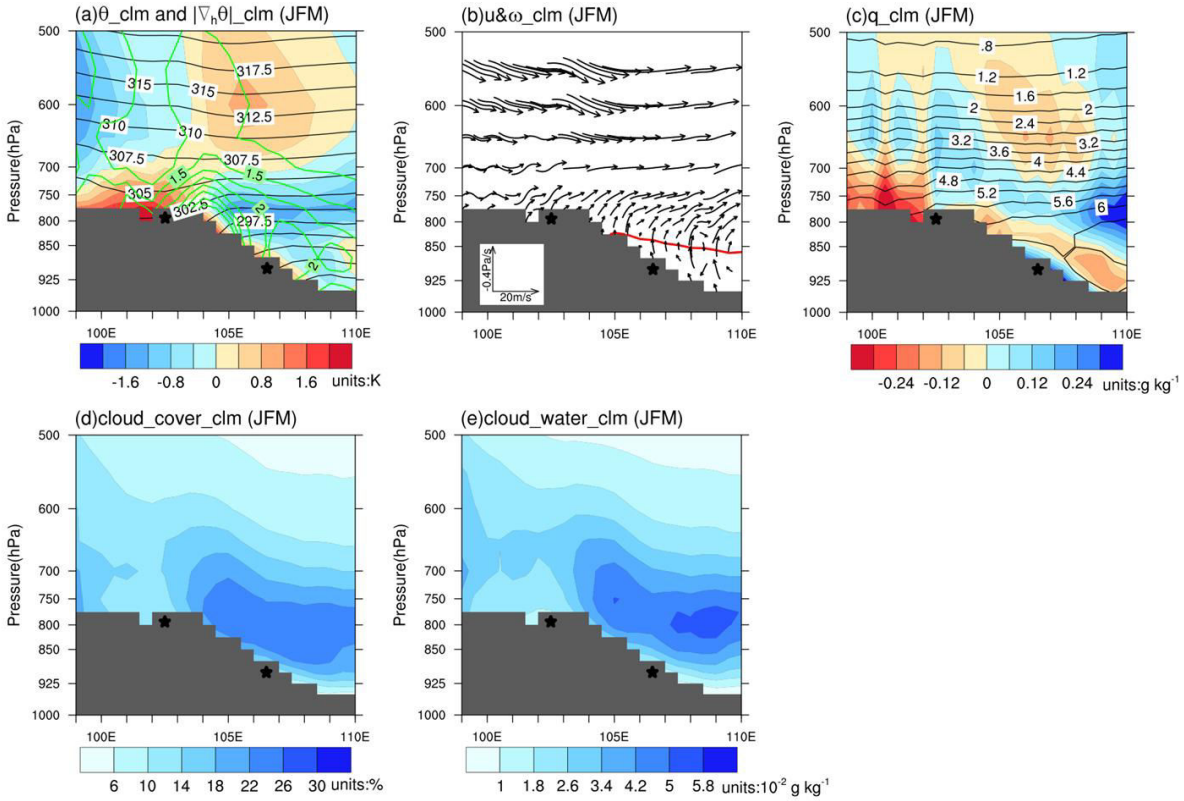

Figure 5 Longitude-altitude sections averaged between 23.5°N-27°N of climatological (a) air potential temperature (black contour, units: K) and its deviation from the zonal mean between 99°E-110°E (shaded, units: K), and horizontal air potential temperature gradient (green contour, units: 10^{-2} K km^{-1}), (b) zonal and vertical wind vector (vector, units: m s^{-1}), (c) specific humidity (contour, units: g kg^{-1}) and its deviation from the zonal mean between 99°E-110°E (shaded, units: g kg^{-1}), (d) fraction of cloud cover (shaded, units:%), and (e) specific cloud liquid water content (shaded, units: 10^{-2} g kg^{-1}) over the Yunnan-Guizhou Plateau, during JFM for 1981-2016. The red line in (b) represents the zero line of climatological zonal wind velocity. The gray shadings represent the topography, and the western and eastern black asterisks represent the location of Kunming and Guiyang, respectively.

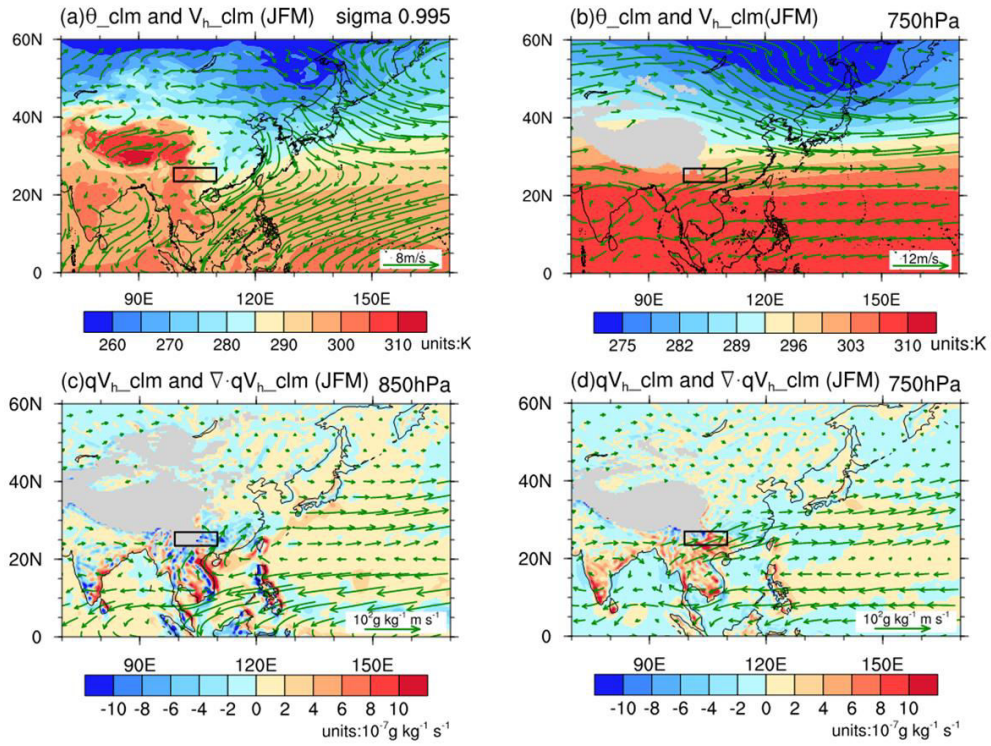

682

683 **Figure 6** Horizontal distributions of climatological air potential temperature (shaded,

684 units: K) and horizontal wind vector (vector, units: m s^{-1}) at (a) the level of sigma

685 0.995 and (b)750 hPa, as well as specific humidity flux (vector, units: 10^2 g kg^{-1} m s^{-1})

686 and its divergence (shaded, units: 10^{-7} g kg^{-1} s^{-1}) at (c) 850 hPa and (d) 750 hPa over

687 East Asia, during JFM for 1981-2016. The black boxes represent the location of the

688 Yunnan-Guizhou Plateau.

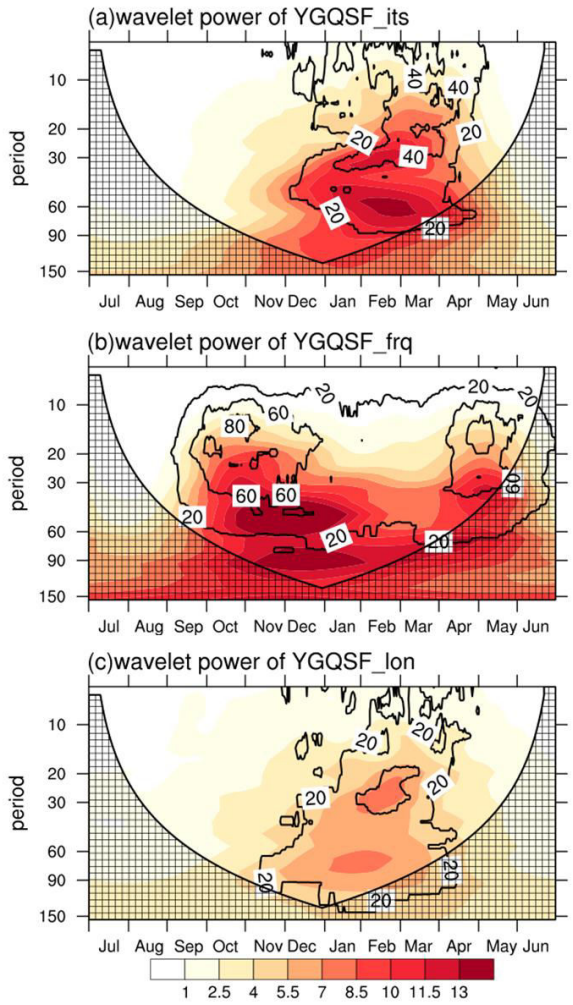

689

690 **Figure 7** Wavelet power spectrum (shaded) averaged from 1981 to 2016 and
691 occurrence ratios (contours, units: %) of the wavelet power exceeding 90%
692 confidence level (regular chi-square test) in 1981-2016 for standardized (a) intensity
693 index, (b) frequency index, and (c) location index of YGQSF. The square-filled
694 shadings are the cones of influence.

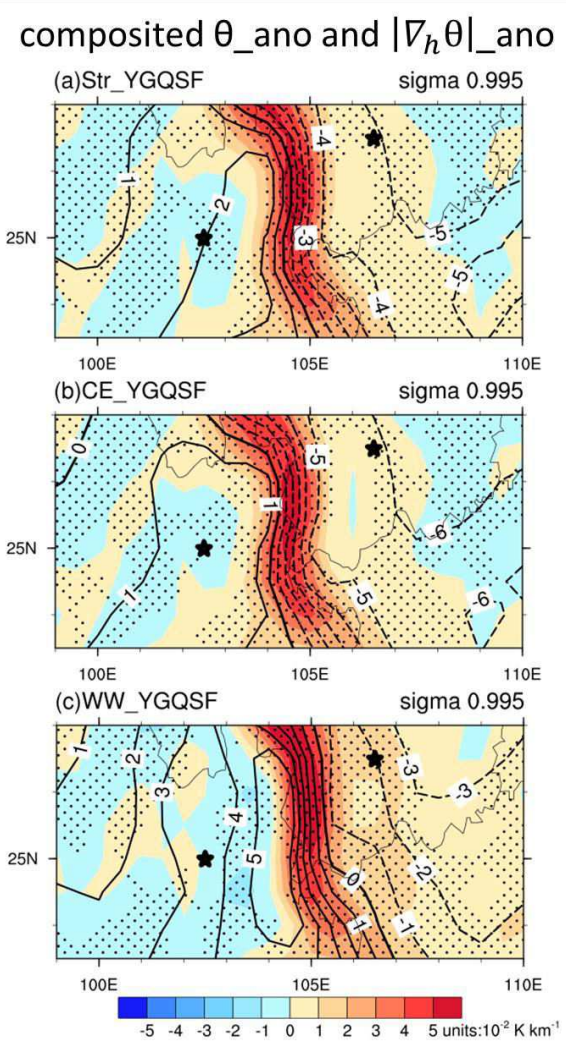

695

696 **Figure 8** Horizontal distributions of composite anomalies of air potential temperature
697 (contour, units: K) and its horizontal gradient (shaded, units: 10^{-2} K km^{-1}) for (a)
698 Str_YGQSF, (b) CE_YGQSF, and (c) WW_YGQSF at the level of sigma 0.995 over
699 the Yunnan-Guizhou Plateau. The dots indicate the regions exceeding 95% confidence
700 level with the Student's t-test. The left (right) black asterisk represents Kunming
701 (Guiyang), as in Fig. 1..

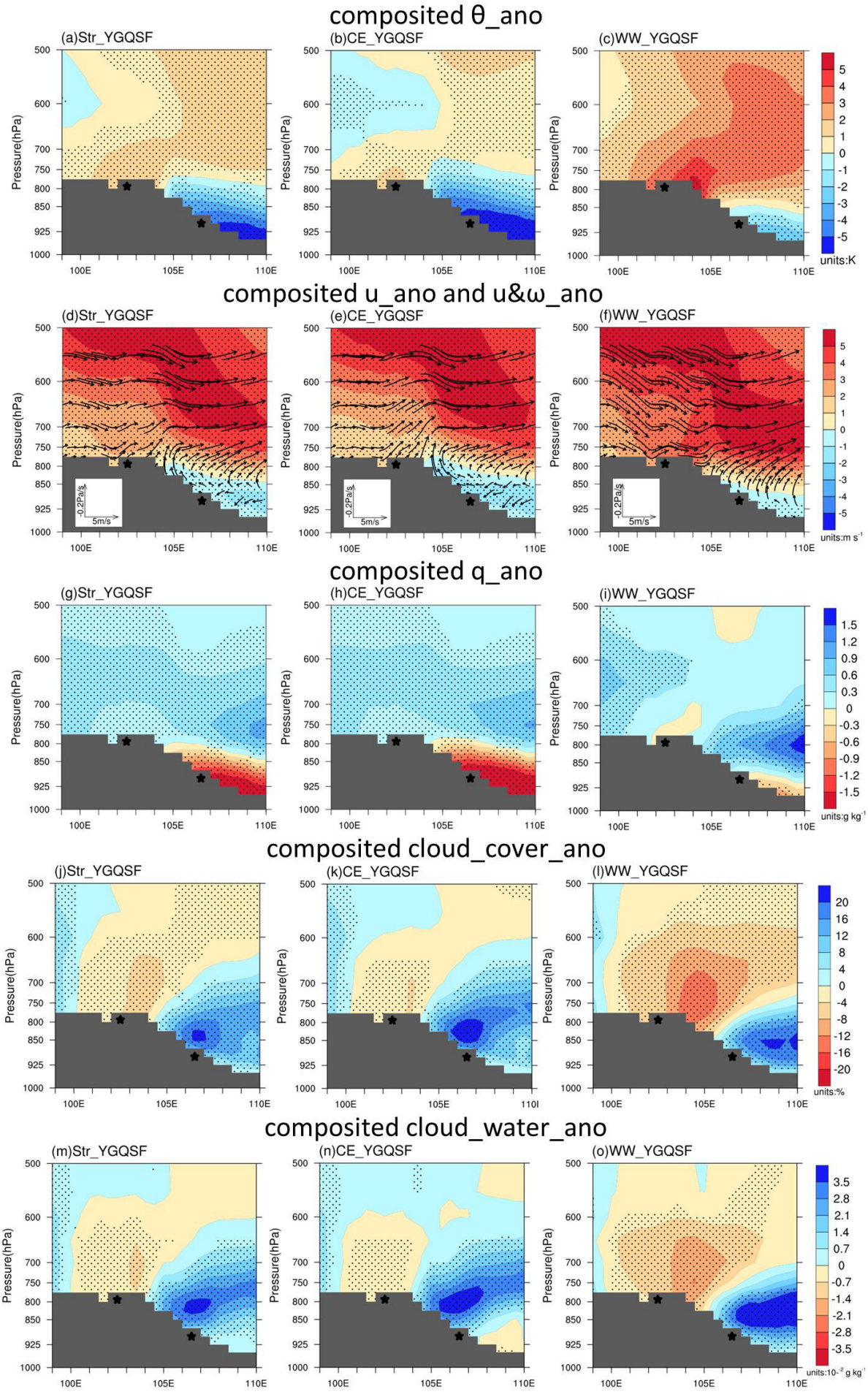
composited θ_ano
(a)Str_YGQSF
(b)CE_YGQSF
(c)WW_YGQSF
composited u_ano and u&ω_ano
(d)Str_YGQSF
(e)CE_YGQSF
(f)WW_YGQSF
composited q_ano
(g)Str_YGQSF
(h)CE_YGQSF
(i)WW_YGQSF
composited cloud_cover_ano
(j)Str_YGQSF
(k)CE_YGQSF
(l)WW_YGQSF
composited cloud_water_ano
(m)Str_YGQSF
(n)CE_YGQSF
(o)WW_YGQSF
Pressure(hPa)
500
600
700
750
800
850
925
1000
100E
105E
110E
5
4
3
2
1
0
-1
-2
-3
-4
-5
units:K
-0.2Pa/s
5m/s
units:m s-1
1.5
1.2
0.9
0.6
0.3
0
-0.3
-0.6
-0.9
-1.2
-1.5
units:g kg-1
20
16
12
8
4
0
-4
-8
-12
-16
-20
units:%
3.5
2.8
2.1
1.4
0.7
0
-0.7
-1.4
-2.1
-2.8
-3.5
units:10-2 g kg-1

Figure 9 Longitude-altitude sections averaged between 23.5°N-27°N of composite anomalies of (a, b, c) air potential temperature (shaded, units: K), (d, e, f) zonal wind velocity (shaded, units: m s^{-1}) and zonal and vertical wind vector (vector, units: m s^{-1}), (g, h, i) specific humidity (units: g kg^{-1}), (j, k, l) fraction of cloud cover (units: %), and (m, n, o) specific cloud liquid water content (units: 10^{-2} g kg^{-1}) for Str_YGQSF (left panels), CE_YGSQF (central panels), and WW_YGQSF (right panels), respectively. The dots indicate the regions exceeding 95% confidence level with the Student's t-test.

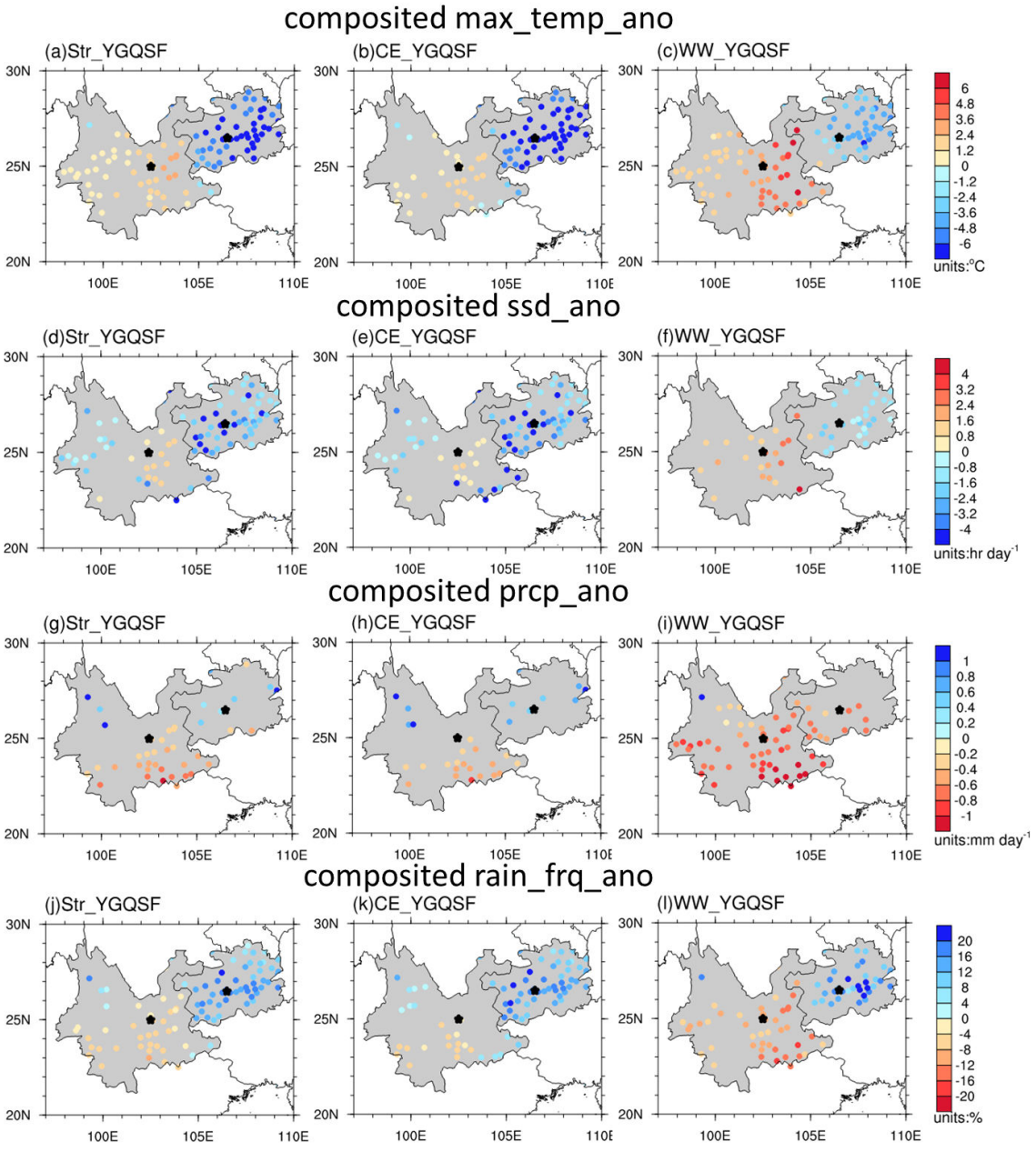

Figure 10 Horizontal distributions of composite anomalies of (a, b, c) daily maximum air temperature (units: ^{o}C), (d, e, f) daily sunshine duration (units: hr day^{-1}), (d, h, i) daily precipitation (units: mm day^{-1}), and (j, k, l) rainfall frequency (units: %) for Str_YGQSF (left panels), CE_YGQSF (central panels), and WW_YGQSF (right panels) in Yunnan and Guizhou Provinces, based on the station records. Note that only the values exceeding 95% confidence level with the Student's t-test are plotted.

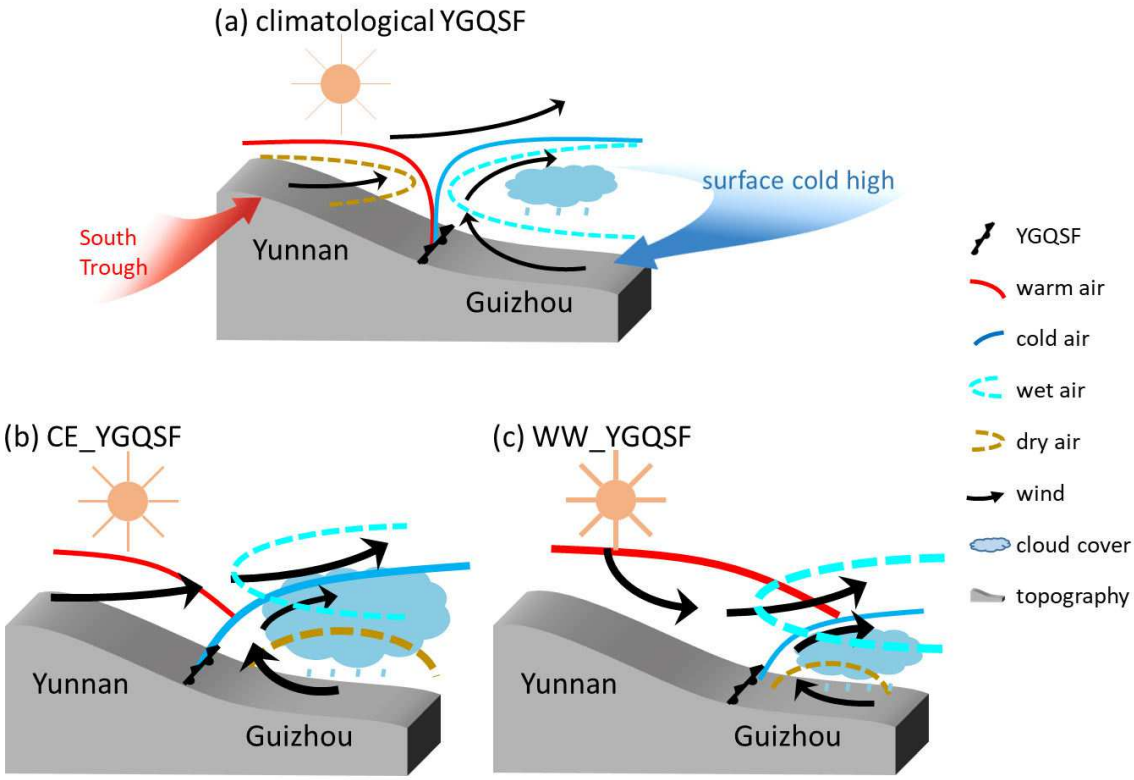

718

719 **Figure 11** Schematic diagrams for the structures of (a) climatological YGQSF, (b)

720 CE_YGQSF, and (c) WW_YGQSF.